Burning of Algae-Derived Biofuel Droplets and Their Mixtures with Jet Fuel

Yuhao Xu,[†] Jordan D. Brunson,[‡] C. Thomas Avedisian,*,[‡] Yiren Shen,[‡] Ivan Keresztes,[§] Anthony M. Condo, Jr.,[§] and Daniel Phillips[||]

[†]Department of Mechanical Engineering, Prairie View A&M University, Prairie View, Texas 77446, United States

[‡]Sibley School of Mechanical and Aerospace Engineering, and [§]Department of Chemistry and Chemical Biology, Cornell University, Ithaca, New York 14853, United States

[||]Backcourt Fuels, LLC., 23501 Cinco Ranch Blvd, Ste H120-129, Katy, Texas 77450, United States

ABSTRACT: This paper reports new results about the combustion dynamics of hydroprocessed renewable jet fuel droplets derived from heterotrophic algae (AHRJ) burning under conditions that promote one-dimensional transport dynamics and near spherically symmetric burning conditions. Results are compared between Jet-A and three AHRJ/Jet-A mixtures containing 25, 50, and 75% AHRJ by volume. The results show that AHRJ droplets burn slightly faster than Jet-A and have a significantly reduced sooting propensity. Detailed chemical analysis also shows that AHRJ contains virtually no aromatics while the aromatic content of Jet-A was 16% by volume. The influence of composition on the burning rate is explained using a simple scaling argument that illustrates the importance of liquid density and other properties.

1. INTRODUCTION

Biofuels produced using algae as the feedstock have potential to reduce particulate emissions because of their minimal aromatic content and to reduce petroleum consumption by volume displacement when blended with conventional petroleum-based fuels such as gasoline and diesel. Most previous studies on algal biofuels have included production technologies[1−3] and life-cycle analysis[4−6] to evaluate the energetic viability of algae as a biofuel feedstock. Very little work has been reported on the fundamental end-use combustion characteristics of blends of algal biofuels with petroleum fuels. The prior work provides more of a system-level perspective of performance in specific engines or from aircraft flight testing protocols.[7−10]

Algal biofuels and the petroleum fuels with which they are mixed are exceedingly complex systems. They comprise hundreds of organic liquids with wide ranges of boiling points and other thermophysical properties. A detailed predictive capability of the combustion processes and influence of the algal biofuel mixture fraction on the fuel burn rate and the environmentally important aspect of formation of particulate matter and gaseous emissions does not exist. In an attempt to build such an understanding to develop the foundation of a predictive capability, this study employs a combustion configuration that is particularly suited to providing access to the basic physics of the algal fuel burning process while still retaining some important elements found in more complex fuel configurations.

Liquid fuels are injected into combustion systems in the form of sprays. However, spray flames are currently too complex to model. This complexity is derived from the turbulent and swirling action of the surrounding gases along with interactive effects of the constituent droplets[11] which constitute the subgrid element of a spray. A fuel burning configuration that eliminates this transport complexity is more advantageous. A spherically symmetric droplet burning configuration serves that purpose. Figure 1 shows this configuration.
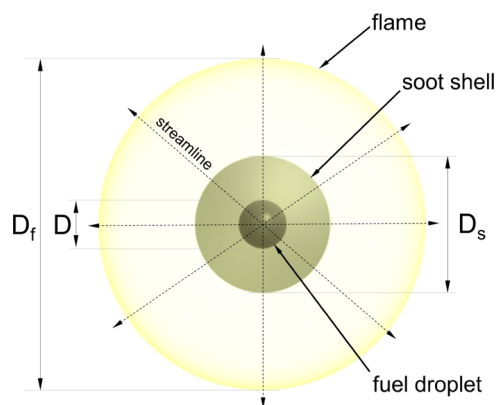
Figure 1. Schematic of a spherically symmetric droplet burning configuration.

The gas flow promoted in this condition is entirely the result of fuel vaporization, and streamlines are radial around the droplet that ostensibly results in a spherically symmetric burning process. Soot aggregates collect in a spherical pattern because of forces acting on them (evaporative flow and thermophoresis).

This base case or canonical configuration of liquid fuel combustion is ideally suited to examine the complexities of burning algal biofuel mixtures because of the simplicity of the
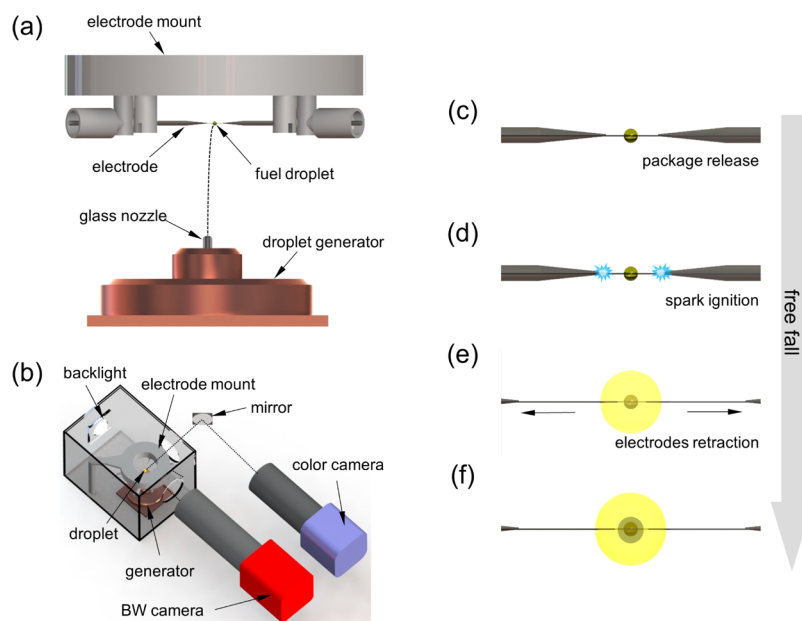
Figure 2. Schematic of the experimental setup: (a) droplet deployment process, (b) layout for two cameras and the combustion chamber inside the instrumentation package, (c—f) sequence of the ignition of a fuel droplet, the retraction of spark electrodes, and the burning of a spherical droplet.

transport process it brings to this otherwise complex problem. Recent studies have successfully simulated the burning characteristics of the spherically symmetric case,[12−18] and it is currently the only liquid phase burning configuration amenable to direct numerical simulation that incorporates the effects of detailed combustion chemistry, preferential vaporization at the interface, moving boundary effects due to fuel evaporation at the droplet surface, transient gas and liquid transports, variable fuel properties, flame radiation, property dependencies on temperature and composition, formation of particulate matter (i.e., soot), and phase equilibrium dynamics which are relevant to miscible mixtures. Data obtained from the configuration of Figure 1 have proven to be valuable for validating comprehensive models of droplet burning and for providing new insights into the controlling mechanisms involved. The data include the time-dependence of the droplet diameter (D), flame diameter (D_f), fuel burn rate (K), and, if soot forms, the soot shell diameter (D_s). Though the present study addresses the algal biofuel burning problem from this experimental perspective, the resulting data will be essential in future work concerning development of ab initio simulations of algal fuel combustion.

To the authors' knowledge, the only prior study of droplet burning of a fuel derived from algae under conditions like those shown in Figure 1 concerned hydrotreated renewable diesel fuel derived from algae.[19] It was found that diesel fuel mixed with renewable algal ("green") biofuel had almost identical burn rates and significantly reduced particulate emissions. The present study concerns blending jet fuel with hydroprocessed renewable jet fuel droplets derived from heterotrophic algae (AHRJ).

Hydroprocessed fuel conventionally refers to a fuel produced from animal fat or vegetable oils.[20] Heterotrophic algae is an attractive strain that can thrive in both the presence and absence of light and CO_2 is not needed for production.[21−26] Varying the mixture fraction of the binary system for the fundamental spherically symmetric config-uration is intended to examine the extent to which the

presence of an algae-based biofuel mixed with jet fuel will alter the dynamics of the fuel burning process.

Experimental data discussed here include the evolutions of droplet, soot shell, and flame diameters. The main parameter is composition. The initial droplet diameter was kept within a relatively small range of 0.5 to 0.6 mm so that this variable was not thought to influence the burning process. The experimental setup and methods are described in Section 2, followed by results and discussions in Section 3 that include chemical analysis of the fuel systems examined, and conclusions in Section 4.

2. EXPERIMENTAL METHODS

2.1. Apparatus. Near spherical droplet flames were developed by carrying out the experiments under conditions where buoyancy and forced convection effects are eliminated. Burning in a reduced gravity environment (order of 10^{-4} of Earth's normal gravity) reduces buoyant flows, and anchoring droplets onto tiny fibers eliminates forced flow effects. "Small" droplets with initial droplet diameters between 0.55 and 0.59 mm as examined here further contribute to minimizing forced and buoyant flow effects (i.e., small Rayleigh and Reynolds numbers).

A schematic of the hardware layout and a sequence of experimental operations are shown in Figure 2. Additional details are given in refs 27−30. Droplets of the desired size were deployed onto the intersection of two SiC fibers (~14 μm diameter) crossed at an angle of approximately 60°. A piezoelectric generator was utilized to deploy the droplets onto the support fibers as shown in Figure 2a. Previous studies showed that droplet support fibers of the size employed in the present study minimally influence burning.[28]

Experiments were carried out under free-fall conditions over a distance of 7.6 m giving an experimental time of about 1.2 s which was sufficiently long to record the complete droplet burning history. During the free-fall, droplets were ignited by two sparks generated across two pairs of retractable electrodes positioned on opposite sides of the droplets (Figure 2d). The sparks were activated about 320 ms after package release to eliminate the effects on initial shaking of the package on the droplet burning. The spark duration was approximately 600 μs, after which the electrodes were rapidly retracted (Figure 2e). The spark parameters were set so that the minimum ignition energy was used for each fuel system examined.
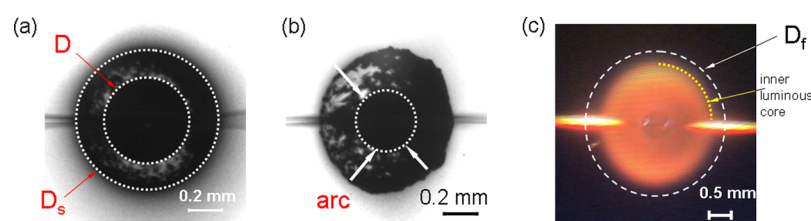
Figure 3. Illustration of size measurements for (a) D and D_s as determined by manual positioning of a virtual ellipse, (b) D as guided by three visible segments, indicated by three arcs, of the droplet boundary, and (c) D_f for a droplet flame.

Table 1. Selected Properties of Fuels Examined

property	Jet-A (POSF 4658)	RJ25	RJ50	RJ75	AHRJ
formula	$C_{10.174}H_{19.913}$[33]				$C_{11.5}H_{25}$[4]
stoichiometric coefficient, ν^a	15.15				17.75
molecular weight, MW (g/mol)	142.3				163.3
H/C ratio (mol)	1.96				2.17
boiling point (bp, K)	478−573[34]				421−573[42]
liquid density, ρ_L (kg/m^3)^b	800	788	775	762	749
lower heating value (kJ/kg)	43 150[4]				43 200[4]
burning rate, K (mm^2/s)^c	0.56	0.57	0.59	0.62	0.63

^{a}Stoichiometric coefficients were calculated assuming 1 mol of fuel and products of CO_2 and H_2O. ^{b}Densities were measured at room temperature using a digital density meter (Mettler Toledo DA-100M). ^{c}Burning rates of Jet-A/AHRJ systems were estimated from Figure 7 by a linear fit of the data from 0.40 to 1.50 s/mm^2.

Doing so provided a fixed initial condition. The time sequences of package release, spark ignition, and electrode retraction are coordinated by a multichannel digital signal generator (Quantum Composer, QC-9618). Ignition was achieved with the minimum spark energy to just ignite the droplets.

The droplet burning process was recorded by a high-speed black and white (BW) camera (Canadian Photonic Labs, Inc., MS-80K, 2320 × 1722 pixel/frame), fitted with an Olympus Zuiko 90 mm f/2.0 lens, an Olympus OM telescopic extension tube 65−116 mm (fixed at 100 mm), and a Vivitar MC 2× teleconverter, which was operated at 200 frames per second to record backlit images that showed droplet and sooting dynamics. A color camera (Hitachi, HV-C20, 640 × 480 pixel/frame, 30 fps), mounted with a Nikkor 135 mm f/2.0 lens and two Kenko 36 mm extension tubes, provided self-illuminated flame images.

It should be noted that the diagnostics employed in the present study are well suited to determining the droplet burning rate, flame structure, and qualitative sooting tendencies, which are the foci of the quantitative information provided by the experiments. However, the optical diagnostics used do not provide information on greenhouse gas emissions (e.g., CO_2).

2.2. Data Extraction. Data were extracted from individual video frames either by an automated algorithm[31] or a manual process using a commercial software package (Image-Pro Plus v6.3, Bethesda, MD). The former was used when the droplet field was relatively free of soot while a manual approach was used for the droplet visibility through the soot cloud was poor. For all the flame data a manual approach was used to obtain flame diameters because the flame boundaries were not sharp (cf., Figure 3). Soot sometimes so obscured the droplet that it was difficult to determine the diameter. In such cases, a process noted in ref 19 was used based on identifying at least two points on the droplet boundary where arcs of the droplet could be identified, then constructing the circle from these arcs as shown in Figure 3b.

For flame diameters, the boundary was too diffused to determine in an automated way and a manual approach was used. A virtual ellipse was manually placed around the boundary of each flame image (dotted circles in Figure 3). The height (H) and width (W) of the ellipse were recorded from Image-Pro and the equivalent diameter D was calculated as $D = (H \times W)^{0.5}$.

D, D_s, and D_f obtained from Image-Pro were converted to millimeters using a factor obtained by a 0.794 mm tungsten−carbide

calibration ball (Salem Specialty Ball Company). The calibration ball was photographed after each experiment with the same settings, such as magnification and background lighting conditions, as during the free-fall experiment. The equivalent diameter of the calibration ball in pixels was extracted by manual measurements using Image-Pro software.

The measurement uncertainty arises from the boundary thickness of the video images that define a "transition area" in the outer boundaries of the droplet, soot shell, and flame.[27] The boundary thickness for D, D_s, and D_f in terms of video pixels was approximately 5, 20, and 8 pixels, respectively. The corresponding measurement precision of data extraction operations from images for droplet, soot shell, and flame diameters ranged from ±1.8 to ±5.3, ±4.7 to ±6.2, and ±3.4 to ±6.2%, respectively.

2.3. Fuel Systems and Chemical Analysis. The aviation fuel was supplied by the Wright Patterson Air Force Base (Dayton, OH, USA): Jet-A, designated as "POSF 4658". The AHRJ was provided by Solazyme, Inc. (now TerraVia Holdings, Inc., San Francisco, CA). Mixtures were prepared in-house on a volumetric basis with AHRJ volume fractions of 0.25, 0.50, and 0.75 (denoted as RJ25, RJ50, and RJ75, respectively). Some representative fuel properties are listed in Table 1.

The compositions of Jet-A and AHRJ were determined by gas chromatography−mass spectrometry (GC−MS) analyses using an Agilent Technologies 6890N gas chromatograph (Santa Clara, CA), an Agilent 7683B auto-sampler, and a JEOL (Peabody, MA) GCMate II double-focusing sector mass spectrometer. Nondiluted 0.2 μL fuel samples were injected via a split/splitless inlet that operated in a split flow mode with a 100:1 split ratio. The temperatures of the inlet and the MS transfer line were set to 285 and 290 °C, respectively.

The oven temperature was first maintained at 60 °C for 15 min, then increased to 180 °C at a rate of 1 °C/min, further to 280 °C at a rate of 25 °C/min, and finally maintained at 280 °C for 6 min. The total oven operation time was 145 min. A DB-5 MS + DG capillary column (Agilent Technologies) (30 m × 0.25 mm ID, 0.25 μm film thickness) and a 10 m DuraGuard column section were used in the GC column. Magnetic field sweeps (with 0.32 s scan periods) were used to collect mass spectra data for masses ranging from 28 to 500. The collected data were analyzed with the help of TSSPro 3.0 software (Shrader Analytical and Consulting Laboratories Inc., Detroit, MI) and a NIST Mass Spectral Database version 2.0.

Total ion chromatograms (TICs) of Jet-A and AHRJ are depicted in Figures 4 and 5, respectively. From this information, detailed
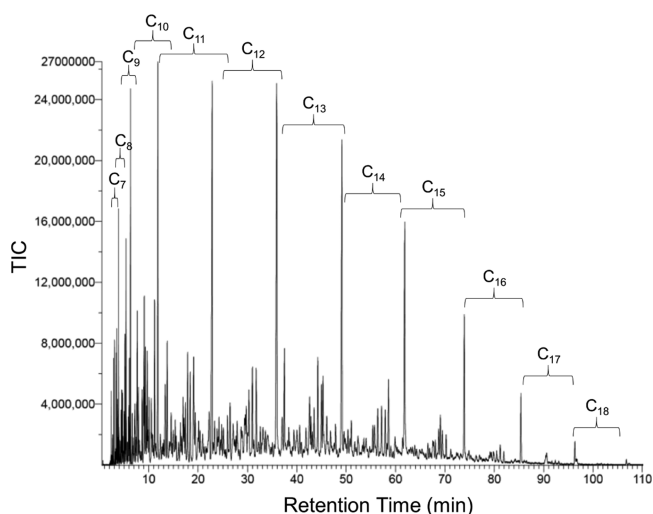

Figure 4. TIC of GC−MS analysis of Jet-A. C_n indicates hydrocarbons with "n" carbon numbers.
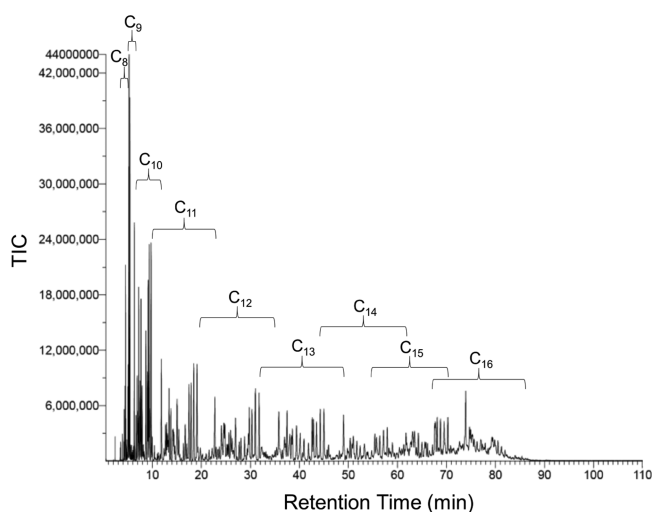

Figure 5. TIC of GC−MS analysis of AHRJ. C_n indicates hydrocarbons with "n" carbon numbers.

compositions of Jet-A and AHRJ were obtained. Results are shown in Tables 2 and 3 for Jet-A and AHRJ, respectively. For each of the compositional groups shown (the first column in Tables 2 and 3) the percent concentrations indicated (e.g., for straight chain, branched, etc.) the sum to 100%.

Table 4 and the pie chart show the concentrations (mole percent) of the major chemical groups in Jet-A and AHRJ. The chemical complexity of Jet-A is evident.

Grouping the constituents as shown above provides information useful for developing surrogates.[32−36] Noteworthy is that Jet-A contains approximately 16% aromatics while AHRJ contains no aromatics. The sooting propensity of AHRJ should therefore be less than Jet-A, and that adding AHRJ to Jet-A should progressively reduce sooting propensity. Experimental results supporting these conjectures are discussed in the next section.

We note that each fractional amount of AHRJ in Jet-A represents essentially a separate system with its own properties and burning characteristics. More specifically, the minimum ignition energy depends on mixture fractions of the components in a fuel blend. Thermal conditions at the start of a burning event are then not necessarily fixed because the energy imparted to the gas surrounding

Table 2. Composition (mol %) of Jet-A Determined by GC−MS

series	total	composition of series				
		straight chain (%)	branched (methyl) (%)	branched (others) (%)	cyclic (%)	aromatics (%)
C_6	trace					
C_7	0.4%					
C_8	1.4%					
C_9	4.2%	23.1	16.9	8.4	34.8	16.8
C_{10}	10.1%	22.5	21.6	14.6	22.6	18.6
C_{11}	18.1%	18.8	16.9	17.8	27.2	19.4
C_{12}	18.4%	20.8	19.3	19.9	21.1	19.0
C_{13}	18.2%	17.4	25.5	15.8	24.5	16.9
C_{14}	14.4%	16.9	28.7	13.8	26.7	13.9
C_{15}	8.7%	15.4	28.7	15.0	30.3	10.5
C_{16}	4.1%	15.1	29.3	14.3	28.7	12.6
C_{17}	1.5%					
C_{18}	0.5%					

Table 3. Composition (mol %) of AHRJ Determined by GC−MS

series	total (%)	composition of series			
		straight chain (%)	branched (methyl) (%)	branched (others)	cyclic
C_8	0.2				
C_9	7.8	13.4	56.7	27.6	2.2
C_{10}	12.4	8.1	50.4	40.7	0.8
C_{11}	12.6	7.2	36.2	56.6	
C_{12}	13.2	9.2	32.4	58.4	
C_{13}	12.6	7.2	31.1	61.7	
C_{14}	8.4	14.0	16.9	69.1	
C_{15}	14.7	12.0	16.9	71.0	
C_{16}	18.0			100.0	

the droplet when the spark is discharged varies with the droplet composition. Some limited numerical work[18] showed the potential for the spark energy itself to influence droplet burning, though more needs to be done on this problem.

3. RESULTS AND DISCUSSIONS

3.1. Flame Structure and Sooting Dynamics. Figure 4 shows a series of color and BW images of burning AHRJ and AHRJ/Jet-A mixture droplets. The photographs for Jet-A come from a prior study[36] and are included for comparison. The first column shows the brightest flame images in the sequences. The indicated times are referenced from the ignition point.

The flames consist of bright yellow cores because of soot incandescence and fainter outer blue zones. The two bright horizontal needle-like glows seen on both sides of the flames arise from the flame intersecting the fibers. Flame brightness is a qualitative measure of the sooting propensity.[37] The photographs suggest that sooting propensities are in the order (high to low) of Jet-A > RJ25 > RJ50 > RJ75 > AHRJ as expected because of the fact that AHRJ has no aromatics as noted above. Aromatics have an elemental form similar to the structure of soot which makes them have a higher sooting propensity compared to fuels which do not contain aromatics. For this reason, diluting Jet-A with its 16% aromatic content (Table 4) by AHRJ with 0% aromatics should reduce soot formation which is consistent with the photographs in Figure 6.

Table 4. Broad Compositional Make-Up of Jet-A and AHRJ

|	Straight Chain	Branched (Methyl)	Branched (Others)	Cyclic	Aromatics
Jet-A	18.8%	23.1%	15.8%	26.0%	16.3%
AHRJ	8.1%	27.4%	64.1%	0.4%	0
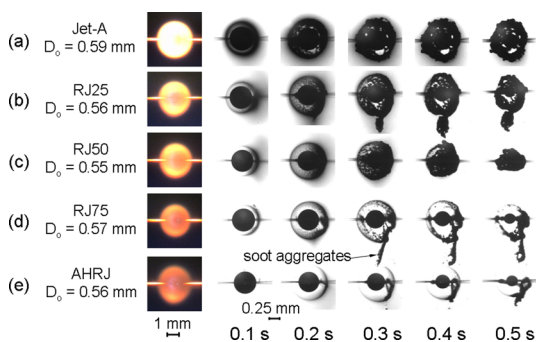
Figure 6. Selected color (maximum illumination) and BW images of (a) Jet-A (D_o = 0.59 mm),[37] (b) RJ25 (D_o = 0.56 mm), (c) RJ50 (D_o = 0.55 mm), (d) RJ75 (D_o = 0.57 mm), and (e) AHRJ (D_o = 0.56 mm). Flame images are selected for maximum illumination in a burning event. Soot clouds are evident in the BW image and show the influence of diluting Jet-A with AHRJ.

The flame luminosity is clearly reduced which is qualitatively indicative of reduced sooting.

The soot "shell" in the BW images is clearly shown in Figure 6. The shell arises when soot aggregates are trapped between the droplet surface and flame by a balance of forces created by thermophoresis and the evaporation-induced flow from the droplet surface. A porous shell structure is formed that gives the appearance of a shell as shown in Figure 6. In some cases, large soot aggregates are formed that cluster around the droplets or outside the shell periphery (e.g., Figure 6b,d at 0.4 s). This effect is not observed in the early period of burning (cf., images at 0.1 s) where aggregates are very small and more "locked" into the shell. As the aggregates grow, they become more vulnerable to disturbances in the gas phase from various convective flows that may arise. The forces on them are progressively dominated by the outwardly directed evaporation-induced flow and that can lead to aggregates drifting away from the drop. A discussion of this effect is given in ref 38.

3.2. Quantitative Measurements. Figure 7 shows measured evolutions of droplet diameters for AHRJ, Jet-A, and AHRJ/Jet-A mixtures.

Three repetitions were carried out for AHRJ to confirm the repeatability of the experiments. It is evident that adding AHRJ to Jet-A increases the burning rate, K, which is defined as the first derivative of the evolution of $(D/D_o)^2$ with t/D_o^2, or $K = \left| \frac{d(D/D_o)^2}{d(t/D_o^2)} \right|$. K is also time-dependent as shown by the curvature of the evolution of diameter in Figure 7. There are several factors to consider in explaining the time and composition dependencies on the burn rate including the
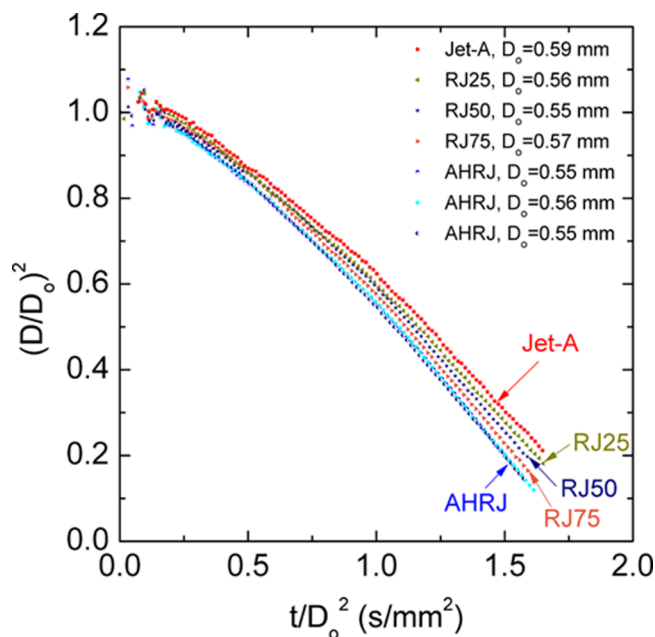
Figure 7. Evolution of the droplet diameter from individual experiments. Multiple experimental runs are included for AHRJ.

role of properties, droplet diameter, soot formation, and flame radiation.

It is known[39] from the classical theory of droplet burning that $K \propto \frac{k_g / C_{pg}}{\rho_L}$ where k_g, C_{pg}, and ρ_L are gas thermal conductivity, gas specific heat, and liquid density, respectively. For a weak dependence of gas properties on temperature, liquid density dominates so that increasing the droplet temperature during the droplet heating period should increase the burn rate because of the decreasing density with increasing temperature. This trend is consistent with Figure 7.

The role of droplet diameter on soot formation comes through the transit or "residence" time, t_r, of fuel molecules from the droplet surface to the flame. It has been shown[40] that $t_r \propto D^2$. As D decreases, the reduced t_r reduces fuel pyrolysis and less soot forms. The photos in Figure 6 generally show this trend. Less soot formation implies that more fuel reaches the flame without pyrolyzing, the flame temperature is higher, more energy is transferred to the droplet, and K increases as burning progresses.

Flame radiation can also influence soot formation through its effect on flame temperature. Large droplets (e.g., >2 mm diameter such as studied on the International Space Station[30]) have correspondingly large flames and significant radiative losses that can lower the flame temperature to where soot formation will actually be reduced. However, radiation as a flame heat loss mechanism is not important for the ∼0.5 mm diameter droplets reported in this paper.

During burning, fuel evaporation decreases the diameter of the drop faster than the flame can adjust to the changing conditions so that the relative position of the flame to the drop increases. This trend is shown in Figure 8 which shows the relative diameter of the flame to the droplet, D_f/D (the flame standoff ratio, FSR), for the various AHRJ/Jet-A mixtures examined. Similarly, the relative position of the soot shell to the droplet, D_s/D (the soot shell standoff ratio, SSR) tracks with the changing flame position as shown by the SSR in figure Figure 8.

933
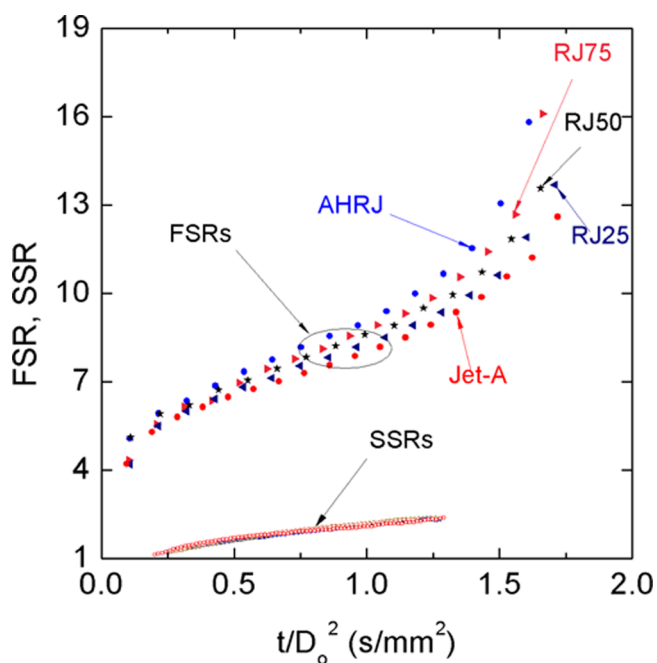
Figure 8. Evolution of flame and soot standoff ratios for the AHRJ/Jet-A blends examined.

A simplified analysis showing the relationship of the FSR to fuel properties was developed in ref 41 that can be put in the form

$$\Theta_{FSR} \equiv \left(\frac{\rho_{L,AHRJ}}{\rho_{L,Jet-A}}\right)\left(\frac{K_{AHRJ}}{K_{Jet-A}}\right)\left(\frac{\nu_{AHRJ}}{\nu_{Jet-A}}\right)\left(\frac{MW_{Jet-A}}{MW_{AHRJ}}\right) \quad (1)$$

where ν is the stoichiometric coefficient with the assumption of a complete combustion and MW is the molecular weight. With property values from Table 1, $\Theta_{FSR} \approx 1.08$ shows that AHRJ should have a slightly higher FSR than Jet-A. This result is consistent with the data in Figure 8 as Jet-A is progressively diluted with AHRJ.

4. CONCLUSIONS

The droplet burning characteristics of a renewable jet fuel derived from algae and three AHRJ/Jet-A blends were compared to conventional aviation fuel—Jet-A—for the base case of droplet combustion in an environment that promotes spherical droplet flames. From the experimental results, AHRJ and AHRJ/Jet-A mixture droplets have burning rates that are higher than Jet-A. Liquid density and soot formation are considered important factors that affect the burning rate. AHRJ/Jet-A mixture droplet flames were positioned further away from the droplet surface than Jet-A droplet flames.

The sooting propensities are in the order of (high to low) Jet-A > RJ25 > RJ50 > RJ75 > AHRJ, which is consistent with the fuel chemical analysis reported that show virtually no aromatics in AHRJ. Correspondingly, Jet-A has the brightest flame because of incandescence of soot particles as they enter the droplet flame region.

The results presented show that the spherically symmetric droplet combustion configuration provides a useful platform to compare the burning characteristics of complex algae-derived biofuels and conventional transportation fuels. The experimental results suggest that AHRJ can be an attractive additive to petroleum-based aviation fuels.

■ AUTHOR INFORMATION

Corresponding Author
*E-mail: cta2@cornell.edu.

ORCID ⊙
C. Thomas Avedisian: 0000-0003-1343-584X

Notes
The authors declare no competing financial interest.

■ REFERENCES

(1) Bala, D. D.; Chidambaram, D. Production of renewable aviation fuel range alkanes from algae oil. *RSC Adv.* **2016**, *6*, 14626−14634.
(2) Batan, L.; Quinn, J.; Willson, B.; Bradley, T. Net Energy and Greenhouse Gas Emission Evaluation of Biodiesel Derived from Microalgae. *Environ. Sci. Technol.* **2010**, *44*, 7975−7980.
(3) Liu, G.; Yan, B.; Chen, G. Technical review on jet fuel production. *Renew. Sustain. Energy Rev.* **2013**, *25*, 59−70.
(4) Lokesh, K.; Sethi, V.; Nikolaidis, T.; Goodger, E.; Nalianda, D. Life cycle greenhouse gas analysis of biojet fuels with a technical investigation into their impact on jet engine performance. *Biomass Bioenergy* **2015**, *77*, 26−44.
(5) Handler, R. M.; Canter, C. E.; Kalnes, T. N.; Lupton, F. S.; Kholiqov, O.; Shonnard, D. R.; Blowers, P. Evaluation of environmental impacts from microalgae cultivation in open-air raceway ponds: Analysis of the prior literature and investigation of wide variance in predicted impacts. *Algal Res.* **2012**, *1*, 83−92.
(6) Sills, D. L.; Paramita, V.; Franke, M. J.; Johnson, M. C.; Akabas, T. M.; Greene, C. H.; et al. Quantitative Uncertainty Analysis of Life Cycle Assessment for Algal Biofuel Production. *Environ. Sci. Technol.* **2013**, *47*, 687−694.
(7) Blakey, S.; Rye, L.; Wilson, C. W. Aviation gas turbine alternative fuels: A review. *Proc. Combust. Inst.* **2011**, *33*, 2863−2885.
(8) Hendricks, R. C.; Bushnell, D.; Shouse, D. T. Aviation Fueling: A Cleaner, Greener Approach. *Int. J. Rotating Mach.* **2011**, *2011*, 1−10.
(9) Rahmes, T. F.; Kinder, J. D.; Henry, T. M.; LeDuc, G. F.; Zombanakis, G. P.; Abe, Y.; Lambert, D. M.; Lewis, C.; Juenger, J. A.; Andac, M. G.; Reilly, K. R.; Holmgren, J. R.; McCall, M. J.; Bozzano, A. G. Sustainable Bio-Derived Synthetic Paraffinic Kerosene (Bio-SPK) Jet Fuel Flights and Engine Tests Program Results. *9th AIAA Aviation Technology, Integration, and Operations Conference (ATIO)*, Sep 21−23, 2009, Hilton Head, South Carolina, paper no. AIAA 2009-7002.
(10) Quiñones, M.; Leung, R.; Williams, S. Algae Based Hydroprocessed Fuel Use on a Marine Gas Turbine. *J. Eng. Gas Turbines Power* **2012**, *134*, 122201.
(11) Sadhal, S. S.; Ayyaswamy, P. S.; Chung, J. N. *Transport Phenomena with Drops and Bubbles*; Springer-Verlag: New York, 1997; Chapters 3 and 6.
(12) Farouk, T. I.; Dryer, F. L. On the extinction characteristics of alcohol droplet combustion under microgravity conditions − A numerical study. *Combust. Flame* **2012**, *159*, 3208−3223.

(13) Alam, F. E.; Liu, Y. C.; Avedisian, C. T.; Dryer, F. L.; Farouk, T. I. n-Butanol droplet combustion: Numerical modeling and reduced gravity experiments. *Proc. Combust. Inst.* **2015**, *35*, 1693−1700.

(14) Liu, Y. C.; Alam, F. E.; Xu, Y.; Dryer, F. L.; Avedisian, C. T.; Farouk, T. I. Combustion characteristics of butanol isomers in multiphase droplet configurations. *Combust. Flame* **2016**, *169*, 216−228.

(15) Farouk, T. I.; Xu, Y.; Avedisian, C. T.; Dryer, F. L. Combustion characteristics of primary reference fuel (PRF) droplets: Single stage high temperature combustion to multistage "Cool Flame" behavior. *Proc. Combust. Inst.* **2017**, *36*, 2585−2594.

(16) Dietrich, D. L.; Nayagam, V.; Hicks, M. C.; Ferkul, P. V.; Dryer, F. L.; Farouk, T.; et al. Droplet Combustion Experiments Aboard the International Space Station. *Microgravity Sci. Technol.* **2014**, *26*, 65−76.

(17) Liu, Y. C.; Farouk, T.; Savas, A. J.; Dryer, F. L.; Avedisian, C. T. On the spherically symmetrical combustion of methyl decanoate droplets and comparisons with detailed numerical modeling. *Combust. Flame* **2013**, *160*, 641−655.

(18) Farouk, T. I.; Liu, Y. C.; Savas, A. J.; Avedisian, C. T.; Dryer, F. L. Sub-millimeter sized methyl butanoate droplet combustion: Microgravity experiments and detailed numerical modeling. *Proc. Combust. Inst.* **2013**, *34*, 1609−1616.

(19) Xu, Y.; Keresztes, I.; Condo, A. M., Jr.; Phillips, D.; Pepiot, P.; Avedisian, C. T. Droplet combustion characteristics of algae-derived renewable diesel, conventional #2 diesel, and their mixtures. *Fuel* **2016**, *167*, 295−305.

(20) Klingshirn, C. D.; DeWitt, M.; Striebich, R.; Anneken, D.; Shafer, L.; Corporan, E.; Wagner, M.; Brigalli, D. Hydroprocessed Renewable Jet Fuel Evaluation, Performance, and Emissions in a T63 Turbine Engine. *J. Eng. Gas Turbines Power* **2012**, *134*, 0515606.

(21) Trivedi, J.; Aila, M.; Bangwal, D. P.; Kaul, S.; Garg, M. O. Algae based biorefinery—How to make sense? *Renew. Sustain. Energy Rev.* **2015**, *47*, 295−307.

(22) Bhatnagar, A.; Chinnasamy, S.; Singh, M.; Das, K. C. Renewable biomass production by mixotrophic algae in the presence of various carbon sources and wastewaters. *Appl. Energy* **2011**, *88*, 3425−3431.

(23) Zhou, Y.; Schideman, L.; Yu, G.; Zhang, Y. A synergistic combination of algal wastewater treatment and hydrothermal biofuel production maximized by nutrient and carbon recycling. *Energy Environ. Sci.* **2013**, *6*, 3765.

(24) Zhu, L.; Hiltunen, E.; Shu, Q.; Zhou, W.; Li, Z.; Wang, Z. Biodiesel production from algae cultivated in winter with artificial wastewater through pH regulation by acetic acid. *Appl. Energy* **2014**, *128*, 103−110.

(25) Chisti, Y. Biodiesel from microalgae. *Biotechnol. Adv.* **2007**, *25*, 294−306.

(26) Singh, A.; Nigam, P. S.; Murphy, J. D. Renewable fuels from algae: An answer to debatable land based fuels. *Bioresour. Technol.* **2011**, *102*, 10−16.

(27) Liu, Y. C.; Avedisian, C. T. A comparison of the spherical flame characteristics of sub-millimeter droplets of binary mixtures of n-heptane/iso-octane and n-heptane/toluene with a commercial unleaded gasoline. *Combust. Flame* **2012**, *159*, 770−783.

(28) Liu, Y. C.; Xu, Y.; Avedisian, C. T.; Hicks, M. C. The effect of support fibers on micro-convection in droplet combustion experiments. *Proc. Combust. Inst.* **2015**, *35*, 1709−1716.

(29) Avedisian, C. T.; Callahan, B. J. Experimental study of nonane/hexanol mixture droplet combustion without natural or forced convection. *Proc. Combust. Inst.* **2000**, *28*, 991−997.

(30) Liu, Y. C.; Xu, Y.; Hicks, M. C.; Avedisian, C. T. Comprehensive study of initial diameter effects and other observations on convection-free droplet combustion in the standard atmosphere for n-heptane, n-octane, and n-decane. *Combust. Flame* **2016**, *171*, 27−41.

(31) Dembia, C. L.; Liu, Y. C.; Avedisian, C. T. Automated data analysis for consecutive images from droplet combustion experiments. *Image Anal. Stereol.* **2012**, *31*, 137−148.

(32) Dooley, S.; Won, S. H.; Chaos, M.; Heyne, J.; Ju, Y.; Dryer, F. L.; Kumar, K.; Sung, C.-J.; Wang, H.; Oehlschlaeger, M. A.; Santoro, R. J.; Litzinger, T. A. A jet fuel surrogate formulated by real fuel properties, Comb. *Flame* **2010**, *157*, 2333−2339.

(33) Pitz, W. J.; Mueller, C. J. Recent progress in the development of diesel surrogate fuels. *Prog. Energy Combust. Sci.* **2011**, *37*, 330−350.

(34) Humer, S.; Seiser, R.; Seshadri, K. Experimental Investigation of Combustion of Jet Fuels and Surrogates in Nonpremixed Flows. *J. Propul. Power* **2011**, *27*, 847−855.

(35) Seshadri, K.; Frassoldati, A.; Cuoci, A.; Faravelli, T.; Niemann, U.; Weydert, P.; Ranzi, E. Experimental and kinetic modeling study of combustion of JP-8, its surrogates and components in laminar premixed flows. *Combust. Theor. Model.* **2011**, *15*, 569−583.

(36) Liu, Y. C.; Savas, A. J.; Avedisian, C. T. Spherically symmetric droplet combustion of three and four component miscible mixtures as surrogates for Jet-A. *Proc. Combust. Inst.* **2013**, *34*, 1569−1576.

(37) Mueller, C. J.; Martin, G. C. Effects of Oxygenated Compounds on Combustion and Soot Evolution in a DI Diesel Engine:Broadband Natural Luminosity Imaging. *SAE Technical Paper*, 2002 2002-01-1631 (2002).

(38) Jackson, G. S.; Avedisian, C. T. Modeling of Spherically Symmetric Droplet Flames Including Complex Chemistry: Effect of Water Addition on n-Heptane Droplet Combustion. *Combust. Sci. Technol.* **1996**, *115*, 125−149.

(39) Turns, S. R. *An Introduction to Combustion*, 2nd ed.; McGraw-Hill: New York, 2000; p 391.

(40) Jackson, G. S.; Avedisian, C. T.; Yang, J. C. Observations of soot during droplet combustion at low gravity: heptane and heptane/monochloroalkane mixtures. *Int. J. Heat Mass Transfer* **1992**, *35*, 2017−2033.

(41) Aharon, I.; Shaw, B. D. On the roles of thermal diffusion and distinct binary diffusion coefficients in modeling droplet flame locations in microgravity. *Microgravity Sci. Technol.* **1997**, *10*, 75−85.

(42) Solazyme Inc. *Material Safety Data Sheet*; Solajet, 2014.